

Numerical Study on the Impacts of the Bogus Data Assimilation and Sea Spray Parameterization on Typhoon Ducts

FEI Jianfang^{1*} (费建芳), DING Juli¹ (丁菊丽), HUANG Xiaogang¹ (黄小刚),

CHENG Xiaoping¹ (程小平), and HU Xiaohua² (胡晓华)

¹ Institute of Meteorology and Oceanography, PLA University of Science and Technology, Nanjing 211101

² Mailbox 5111, Beijing 100081

(Received September 24, 2012; in final form March 4, 2013)

ABSTRACT

The Weather Research and Forecasting model version 3.2 (WRF v3.2) was used with the bogus data assimilation (BDA) scheme and sea spray parameterization (SSP), and experiments were conducted to assess the impacts of the BDA and SSP on prediction of the typhoon ducting process induced by Typhoon Mindule (2004). The global positioning system (GPS) dropsonde observations were used for comparison.

The results show that typhoon ducts are likely to form in every direction around the typhoon center, with the main type of ducts being elevated duct. With the BDA scheme included in the model initialization, the model has a better performance in predicting the existence, distribution, and strength of typhoon ducts. This improvement is attributed to the positive effect of the BDA scheme on the typhoon's ambient boundary layer structure.

Sea spray affects typhoon ducts mainly by changing the latent heat (LH) flux at the air-sea interface beyond 270 km from the typhoon center. The strength of the typhoon duct is enhanced when the boundary layer under this duct is cooled and moistened by the sea spray; otherwise, the typhoon duct is weakened. The sea spray induced changes in the air-sea sensible heat (SH) flux and LH flux are concentrated in the maximum wind speed area near the typhoon center, and the changes are significantly weakened with the increase of the radial range.

Key words: atmospheric duct, tropical cyclone, the BDA scheme, sea spray, numerical simulation

Citation: Fei Jianfang, Ding Juli, Huang Xiaogang, et al., 2013: Numerical study on the impacts of the bogus data assimilation and sea spray parameterization on typhoon ducts. *Acta Meteor. Sinica*, **27**(3), 308–321, doi: 10.1007/s13351-013-0303-8.

1. Introduction

It has long been recognized that accurate predictions of electromagnetic (EM) wave propagation in the atmosphere require a knowledge of modified refractivity (M ; in unit of M) profiles (Dockery, 1988), and the modified refractivity M is related to the atmospheric temperature (T ; K), partial pressure of water vapor (e ; hPa), atmospheric pressure (P ; hPa), and the altitude (z ; m) above surface (Bean and Dutton, 1968):

$$M = 77.6 \frac{P}{T} - 5.6 \frac{e}{T} + 3.75 \times 10^5 \frac{e}{T^2} + 0.157z. \quad (1)$$

The four refraction regimes, i.e., subrefraction, normal refraction, superrefraction, and trapping, are each

characterized by a range of M slope values. Ducting or EM trapping occurs when $dM/dz < 0$, which is often associated with sharp decrease of moisture and temperature inversion. Following the definition of Turton et al. (1988), a trapping layer is located inside and at the top of a duct. The duct is defined as the layer in which M is higher than the minimum value at the top of the trapping layer, thus the ducting layer can be thicker than the trapping layer. Trapping layers and ducts are easily identified from the vertical profiles of M . Figure 1 shows the idealized M profiles for several main types of ducts: surface duct (including simple surface duct and S-shaped surface duct), elevated duct, and evaporation duct. Surface duct refers

Supported by the National Natural Science Foundation of China (41230421, 41205004, 41005029, and 41105065) and China Meteorological Administration Special Public Welfare Research Fund (GYHY201106004).

*Corresponding author: feijf@sina.com.

©The Chinese Meteorological Society and Springer-Verlag Berlin Heidelberg 2013

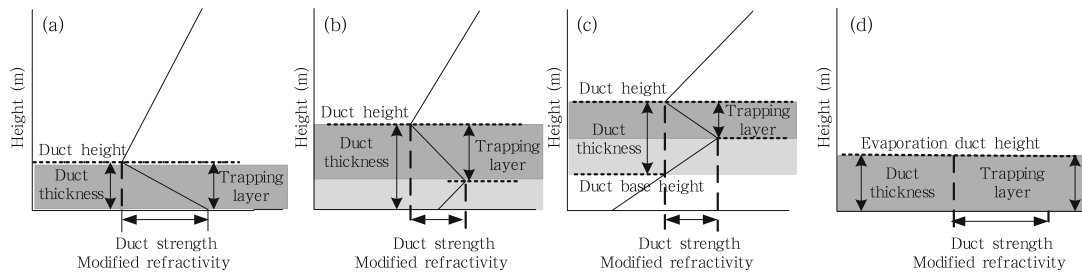


Fig. 1. Typical modified refractivity M profiles for (a) simple surface duct, (b) S-shaped surface duct, (c) elevated duct, and (d) evaporation duct (from Atkinson et al., 2001).

to all ducts that extend down to the land or sea surface, and evaporation duct is actually a subset of the surface duct, which forms just above the sea surface with strong vertical humidity gradient (Cook, 1991). Of course, real M profiles can be a combination of these main types, with multiple ducts coexisting at different levels or several trapping layers inside a same duct (Mesnard and Sauvageot, 2010).

Pan et al. (1996) pointed out that the western and northwestern fringes of a typhoon and the typhoon eye are the favorable places for duct formation. This is because typhoons over the western North Pacific (WNP) usually move around the edge of the subtropical high, where subsidence inversion often appears, and the flows at the western and northwestern fringes of typhoons transport sufficient water vapor under the inversion, while the existence of this inversion inhibits the upward transfer of water vapor, yielding a sharp gradient of moisture. They also indicated that elevated duct layers are likely to form beyond a distance of 1100 km from typhoon centers, whereas those generated in the typhoon eye are usually at the altitude of about 800 m. In October 1997, an experiment was carried out by the China Research Institute of Radio Wave Propagation (CRIRWP) for a month, to explore the tropospheric duct structure on the southeastern coast of China. Based on the observations from this experiment, Liu et al. (2002) reported increased duct frequency on the western periphery of the tropical cyclones (TCs). The associated ducts are usually referred to as TC-Ducts or typhoon ducts, which are likely to form on the periphery of a typhoon and its eye, instead of in the inner core area where intense convection makes temperature and moisture

fully mixed, which is disadvantageous to the formation of temperature inversion and ducts. Chang and Lin (2011) analyzed an unusual radar abnormal propagation (AP) phenomenon associated with foehn winds induced by Typhoon Krosa (2007), and found that subsidence warming generated by downslope winds induced a temperature inversion above the surface and caused the ducting of radar beams.

Despite the above studies, the occurrence of typhoon ducts is still not well documented, since the previous studies are usually based on conventional radiosonde data over land. The coarse vertical resolution of the radiosonde data may smooth out some ducting layers and broaden the thickness of ducts. Moreover, these data are usually obtained over land. The survey of typhoon ducts over oceanic areas is incomplete because the information about ducts in or around typhoons over the sea is unavailable. Owing to the implementation of the “Dropsonde Observation for Typhoon Surveillance near the Taiwan Region (DOTSTAR)” program, more refined structures of temperature and humidity profiles with vertical resolutions of about 5–6 m are revealed through using the global positioning system (GPS) dropsondes in or around typhoons. The DOTSTAR program provides a strong database for studies on the occurrence and structure of typhoon ducts over the sea. Ding et al. (2013) show that typhoon ducts are likely to form in all directions around the typhoon center, with an average distance of about 412.8 km from the center; they occur more frequently and are much stronger in southwest and northwest directions than in the other directions; with the increase of typhoon intensity, the associated ducts inside typhoons tend to be much stronger and thicker

and to appear at higher altitudes. But the following problems remain: the GPS dropsonde data are gathered from single point observations with a coarse spatial resolution, and their deployments are somewhat random relative to the typhoon center; besides, the temporal continuity of the dropsonde observations is limited since one research flight can only last for 3 h or so.

Therefore, it is of great necessity to carry out numerical simulations of typhoon ducts using mesoscale numerical prediction models. Related numerical simulations can also provide early warning for wide-range and long-term typhoon ducts, and help further analyze duct formation causes. Similar studies were conducted by Hu et al. (2007) using the Advanced Regional Prediction System (ARPS) to simulate a ducting process induced by Typhoon Rusa (2002), by Cheng (2009) using the fifth-generation Pennsylvania State University/National Center for Atmospheric Research Mesoscale Model MM5 to simulate a typhoon duct case induced by Typhoon Rammasun (2008), and by Liu et al. (2012) using the Weather Research and Forecasting (WRF) model to investigate the cause of typhoon ducts induced by Typhoon Rusa (2002). It is worth noting that these studies focused on the ducts on the west side of the related typhoons, and did not consider the effect of typhoon intensity.

Our previous study (Ding et al., 2013) indicates that the distribution of typhoon ducts is linked with the variation of typhoon intensity. Therefore, we speculate that improving the simulation of typhoon intensity is conducive to the simulation of typhoon ducts. The bogus data assimilation (BDA) scheme (Xiao et al., 2000; Zou and Xiao, 2000) is recognized to be advantageous to simulation of typhoon intensity. In addition, under high wind conditions such as typhoon, sea spray generated by wave breaking and air bubbles may release spray sensible and latent heat fluxes to the environmental atmosphere, changing the ambient temperature and humidity profiles, as well as the atmospheric refraction field and ambient duct structure. The influences of the BDA and sea spray parameterization (SSP) on typhoon ducts remain a topic that needs a further numerical study.

This paper is arranged as follows. Overview of the selected typhoon duct case is provided in Section 2. Model configuration and design of numerical experiments are presented in Section 3. The impacts of the BDA and SSP on typhoon ducts are discussed in Section 4. A summary and conclusions are given in Section 5.

2. Overview of typhoon ducts

2.1 *Typhoon Mindule*

Mindule was formed as a tropical storm (TS) to the east of the Philippines over the western North Pacific (WNP) at 0600 UTC 23 June 2004. It moved westward and strengthened gradually to a severe tropical storm (STS) at 0600 UTC 24 June, then it kept moving westward and strengthened as a typhoon (TY) at 1200 UTC 27 June with the moving direction changing to northwestward, and it quickly strengthened to a severe typhoon (STY) at 0000 UTC 28 June. Mindule reached its peak intensity at 0000 UTC 29 June with minimum central pressure of 940 hPa and maximum sustained wind speed of 49 m s^{-1} based on the best track data provided by the Japan Meteorological Agency (JMA), and the peak intensity lasted for 12 h. After that, Mindule gradually weakened and made a sudden reversal to northward when moving into the Bass Strait (122°E). At 0230 UTC 1 July, it landed in Hualian, Taiwan Region, and then moved to the south of the East China Sea with its intensity weakened to STS after it traversed the Taiwan Island. At 0130 UTC 3 July, it landed in Leqing, Zhejiang Province, and then moved northward along the coastlines. After transferring to the Zhoushan sea area, it moved northeastward with accelerated speed and weakened intensity. At 0000 UTC 4 July, it became a tropical depression and gradually dissipated. Details of the Mindule's track can be found in Fig. 2a.

2.2 *Typhoon ducts*

From 1036 UTC 27 to 1252 UTC 29 June (Fig. 2b), the DOTSTAR program carried out 3 research flights (once a day at 1200 UTC or so) and deployed 47 GPS dropsondes to investigate Typhoon Mindule

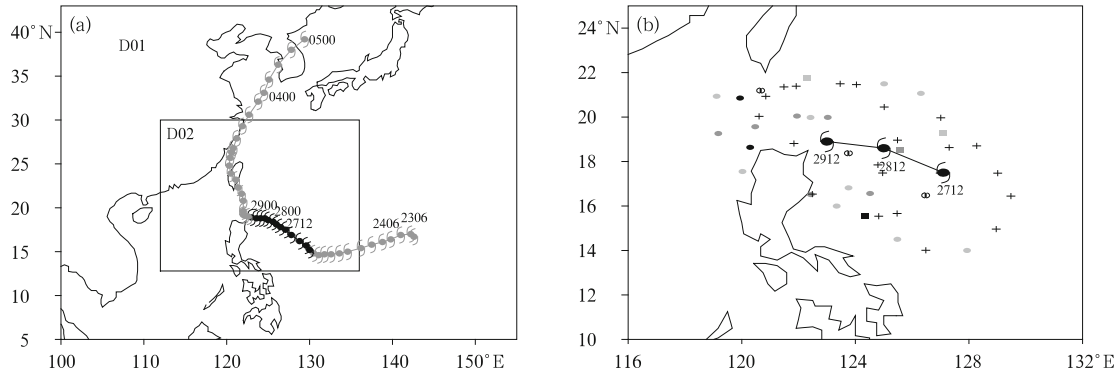


Fig. 2. (a) The best track of Typhoon Mindule (2004) from the JMA data and the model domain configuration. (b) The dropsonde deployment around Mindule as well as the observed duct locations. The typhoon symbol indicates position of the typhoon center. Solid circles indicate dropsonde-derived duct positions with tops less than 1000 m; solid pane indicate duct positions with tops between 1000 and 2000 m; hollow circles with a vertical line in the center indicate duct positions with tops above 2000 m. Black symbolizes strong duct ($\delta M > 10$ M; δM is duct strength); gray symbolizes moderate duct ($5 \text{ M} < M \leq 10 \text{ M}$); shallow gray symbolizes weak duct ($\delta M \leq 5 \text{ M}$). Plus signs indicate the positions of dropsondes with no duct observed.

(2004), of which one dropsonde records are invalid and discarded. Twenty-four cases in the total 46 dropsondes show ducting conditions with its strength larger than or equal to 2 M, among which 10 cases exhibit multiple ducts. Details of the statistical results are shown in Table 1. Note that for profiles with multiple ducting layers, only the strongest ducts are retained.

3. Model configuration and experimental design

The numerical model and data used in this study are the Advanced Research WRF (ARW) version 3.2 and the $1^\circ \times 1^\circ$ NCEP global final analysis at 6-h intervals. The TC best track data provided by the JMA are also used. The WRF model uses fully compressible, Eulerian nonhydrostatic equations with a mass vertical coordinate. The horizontal resolutions of the two domains are 27 (D01) and 9 km (D02) with a two-

way nesting, and the grid dimensions are 226×179 and 247×205 , respectively (as shown in Fig. 2a). There are 49 vertical levels for each domain and the vertical spacing increases with height so as to ensure good resolutions at low altitudes. Specifically, there are 23 levels in the planetary boundary layer (PBL) with resolution of about 15 m at the lowest levels for refined capture of the M profile. The MM5 surface layer (SL) scheme is used in conjunction with the Yonsei University (YSU) (Hong et al., 2006) PBL parameterization. The other physical parameterizations used in this study include the Lin microphysics scheme (Lin et al., 1983; Rutledge and Hobbs, 1984), Noah land-surface model (LSM) described by Chen and Dudhia (2001), Kain-Fritsch (KF) scheme (Kain, 2004; Kain and Fritsch, 1990) for cumulus parameterization, Rapid Radiative Transfer Model (RRTM) for longwave radiative flux computations (Mlawer et al., 1997), and Dudhia scheme (Dudhia, 1989) for shortwave

Table 1. Statistical results of the ducts induced by Typhoon Mindule (2004) based on the GPS dropsonde data

	Position to the typhoon center			
	Northeast	Southeast	Southwest	Northwest
Number of ducts/deployments	2/8	3/9	7/10	12/19
Occurrence percentage (%)	25	33	70	63
Mean distance from typhoon center (km)	314.4	308.6	319.0	401.4
Mean duct strength (M)	2.99	3.12	7.39	5.59
Mean duct thickness (m)	66.9	99.7	115.1	100.6
Mean duct height (m)	585.5	1319.5	550.8	1156.2

radiation.

In this study, three numerical experiments (see Table 2) were designed to evaluate impacts of the BDA and SSP on the ducting process induced by Typhoon Mindule (2004). All the experiments were initialized at 1200 UTC 26 June 2004 and ended at 1200 UTC 29 June 2004. During this period, the DOTSTAR program carried out a three-day observation for Typhoon Mindule (2004), providing valuable measurements to verify the model results. EXP-1 was initialized with $1^\circ \times 1^\circ$ NCEP global final analysis data with the above physical parameterizations. The configuration of EXP-2 is the same as that of EXP-1, except that the EXP-2 initialization used the WRF three-dimensional variational (3DVAR) data assimilation system with the BDA scheme (Xiao et al., 2008).

The BDA scheme was only applied to the coarse grid D01. For D02, all the variables were interpolated from those of D01. The background error covariance was calculated from 1-month statistics during 12 June–12 July 2004 using the NMC (National Meteorological Center) method (Parrish and Derber, 1992). To evaluate the impact of sea spray on typhoon ducts, EXP-3 was conducted, in which the surface interfacial fluxes were calculated from standard MM5 SL scheme in WRF v3.2, whereas the sea spray fluxes were computed by the Fairall parameterization scheme (Fairall et al., 1994). More details were given in Zheng et al. (2008). Since the combination of WRF 3DVAR and the BDA scheme can potentially greatly improve the typhoon intensity forecast, this combination was retained in EXP-3.

Table 2. Summary of numerical experiments

Number	Name	General configuration
EXP-1	YSU_MM5	Initialized by $1^\circ \times 1^\circ$ NCEP global analysis with YSU PBL scheme and MM5 SL scheme
EXP-2	BDA_YSU_MM5	Same as EXP-1, but initialized by WRF 3DVAR with the BDA scheme
EXP-3	BDA_YSU_fair	Same as EXP-2, but with the Fairall et al. (1994) SSP incorporated into the MM5 SL scheme

Note: SL denotes surface layer.

4. Numerical results

4.1 Impact of the BDA scheme

4.1.1 Typhoon intensity

According to the JMA best track data, Typhoon Mindule (2004) was strengthening during 1200 UTC 26–1200 UTC 29 June, and after 1200 UTC 29 June, it started to weaken. As shown in Fig. 3a, both the strengthening process and the late weakening trend of Typhoon Mindule were successfully simulated by EXP-1 and EXP-2. In the first 42 h, EXP-1 failed to predict the minimum sea level pressure (MSLP) with its prediction much weaker than the observation, due to the lack of the bogus vortex assimilation in the model initial field; but after 48 h, the predicted MSLP became much closer to the observation. In comparison, EXP-2 with the BDA scheme in the initialization successfully improved the MSLP prediction in the first 36 h, and the predicted MSLP became a little stronger than the observation in the late period of integration,

but the weakening trend of Typhoon Mindule was still well captured.

In addition to the MSLP, the maximum 10-m wind speed is also used to reflect the typhoon intensity. Figure 3b shows that both experiments are able to simulate the strengthening, maintenance, and the late weakening of Typhoon Mindule, but EXP-2 with the BDA scheme achieved an overall better performance in predicting the maximum 10-m wind speed.

4.1.2 Distribution of typhoon ducts

To evaluate how the improved typhoon intensity affects the prediction of typhoon ducts, we first compare the simulated distributions of typhoon ducts with the dropsonde measurements at 1200 UTC 27 June, when the predicted typhoon intensity from EXP-2 was closest to the observation (Fig. 3). Note that, since the duct with strength less than 2 M may have little impact on EM propagation, in this study, only those with strength larger than or equal to 2 M are considered. As shown in Figs. 4a and 4b, typhoon ducts

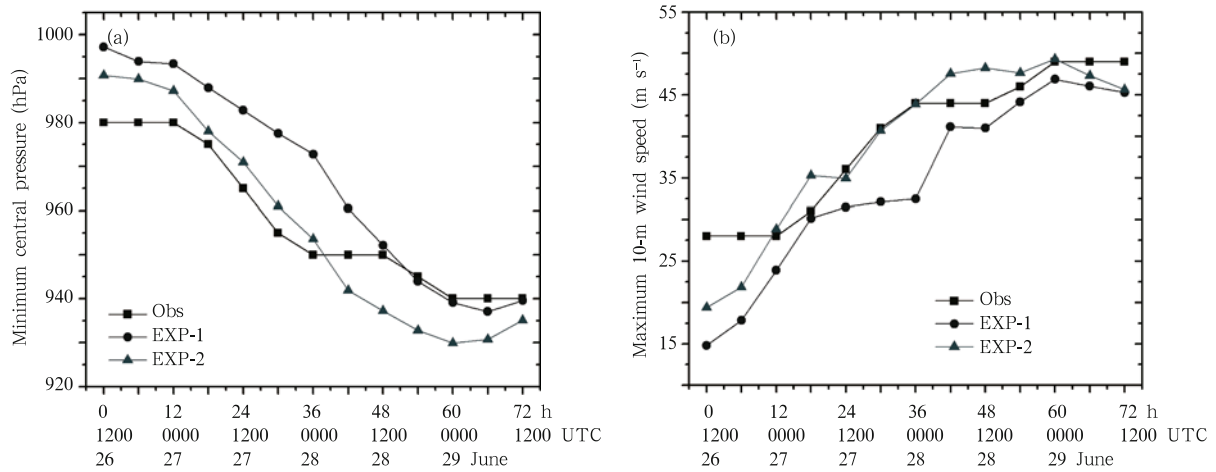


Fig. 3. Time series of (a) minimum sea level pressure (hPa) and (b) maximum 10-m wind speed (m s^{-1}) for Typhoon Mindule (2004) from EXP-1 and EXP-2.

are likely to form in every direction around the typhoon center, with the main type of ducts being elevated duct. In addition, improved typhoon intensity simulation by use of the BDA in the initialization has a great impact on the typhoon duct distributions. At 1200 UTC 27 June (24-h integration), the simulated elevated ducts from both experiments were widely distributed beyond a 300–500 km radius from the typhoon center, whereas the inner boundary of ducts from EXP-2 was more arc-shaped, with a wider duct coverage in the Bass Strait and the northeast side of the Philippines. The empty circles in Fig. 4 indicate dropsonde-derived elevated ducts whereas the solid ones indicate the simulated elevated ducts. Obviously, the simulated distribution of typhoon ducts from EXP-2 is much closer to the observation than that from EXP-1. This means that improved typhoon intensity forecast by the BDA scheme is favorable to the prediction of typhoon duct distributions.

The simulated duct strength and duct height from EXP-1 and EXP-2 are shown in Figs. 4c–4f. It is evident that the simulated ducts with strength larger than 2 M have a wider coverage by introducing the BDA scheme, with their tops at lower altitudes. But with increased distance from the typhoon center, the impacts of the BDA scheme on the simulated duct properties tend to be less effective. It is important to note that, the simulated surface ducts to the south and east of the typhoon center are actually evapora-

tion ducts, which seem not very reliable and are left undiscussed, due to the still poor vertical resolution of the model in the surface layer.

4.1.3 Duct structure

As shown in Fig. 5, improved typhoon intensity simulation by the BDA scheme can also exert a positive effect on the typhoon duct structure. Especially, in Figs. 5a and 5e, EXP-1 failed to simulate the existence of two ducts, but EXP-2 managed to successfully produce them. In Figs. 5b–5d, though both experiments simulated the existence of three ducts, the duct strength simulated by EXP-2 was much closer to the observation. This implies that better typhoon intensity simulation by the BDA scheme is also important for correct simulation of typhoon duct structures. Thus, improving typhoon intensity forecast by the BDA scheme is beneficial to not only distribution (see Section 4.1.2) but also structure forecasts of typhoon ducts.

However, there are still some differences between the model results and the observations, which may be associated with the following reasons. First, the temperature and humidity profiles of the PBL cannot be properly resolved in the model initialization, especially over the sea. Second, the model results are respectively after 23-, 24-, 26-, 47-, and 71-h integration when model errors have been introduced in the integration process. Third, the observations are of a much higher vertical resolution. Despite these disad-

vantages, the forecasting capability of the WRF v3.2 model on typhoon ducts is encouraging.

4.2 Impact of sea spray

4.2.1 Typhoon intensity

Figure 6 gives comparison of Mindule's simulated intensity from EXP-2 and EXP-3 and the JMA best track data. It can be seen that in the first 36 h of the

simulation, the simulated MSLP and maximum 10-m wind speed are very close to the observations in different experiments, with and without sea spray. This is mainly because Mindule is still a little weak though it is gradually strengthening. After 36 h, the impacts of sea spray are significantly enhanced with the development of Mindule, resulting in increased air-sea flux exchange and causing the typhoon system to further

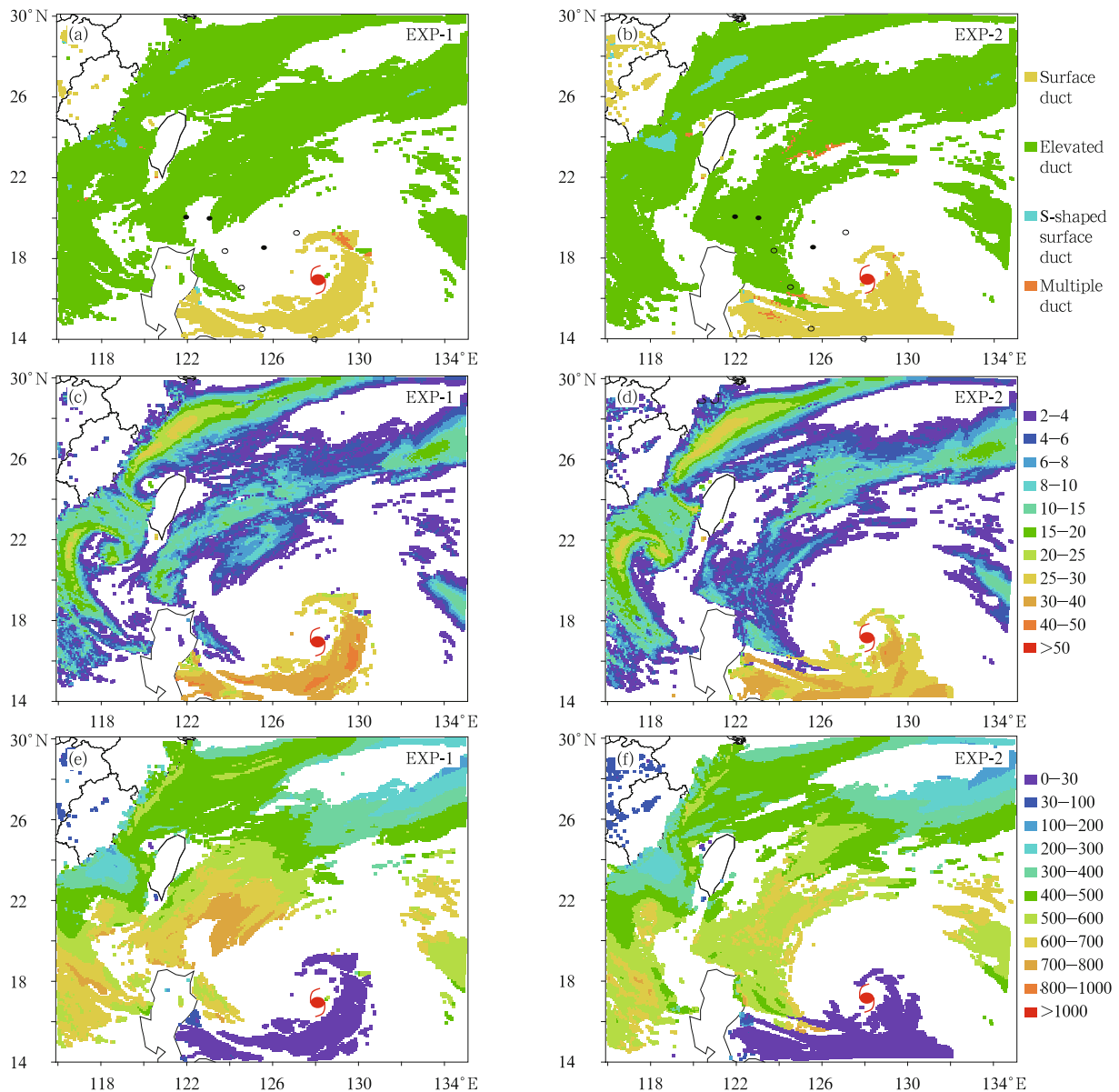


Fig. 4. Horizontal distributions of the simulated (a, b) duct type, (c, d) duct strength in M, and (e, f) duct height in m, from (a, c, e) EXP-1 and (b, d, f) EXP-2 at 1200 UTC 27 June. The typhoon symbol indicates position of the typhoon center; empty circles indicate dropsonde-derived elevated duct positions while solid circles indicate the dropsonde-derived multiple elevated ducts.

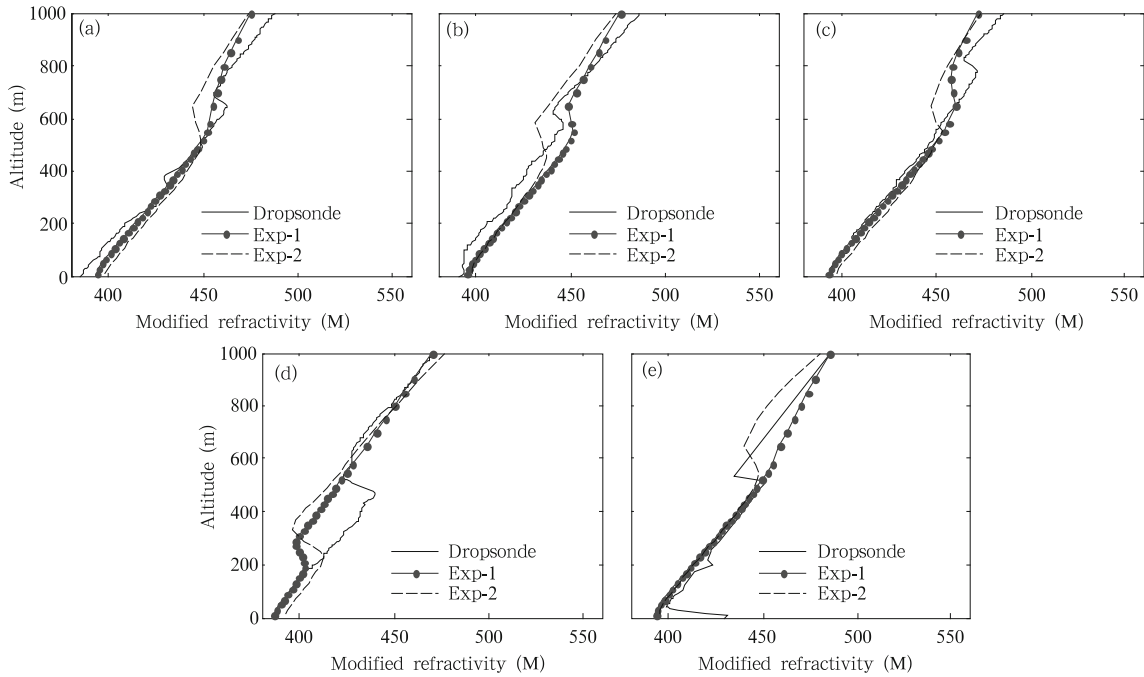


Fig. 5. Vertical profiles of modified refractivity from EXP-1 and EXP-2 versus the GPS dropsonde measurements.

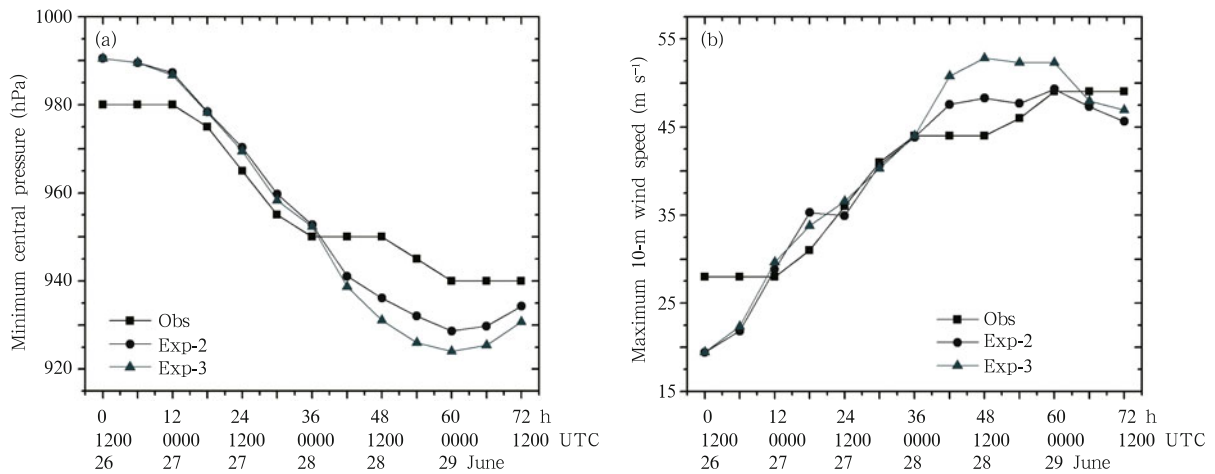


Fig. 6. As in Fig. 3, but for EXP-2 and EXP-3 versus the JMA best track data.

strengthen with accelerated wind speed. In the final 36 h of the simulation, the average reduction of MSLP is 3.8 hPa after taking into account the effect of sea spray, whereas the maximum 10-m wind speed is increased by 2.5 m s⁻¹ on average.

4.2.2 Distribution of typhoon ducts

To emphasize the effect of sea spray on typhoon duct distribution, we analyze the model results with and without SSP at 1200 UTC 28 June when the sea

spray effect was obvious according to Fig. 6. As shown in Fig. 7, the effect of sea spray on typhoon duct distribution is not significant, but is more evident than that at 1200 UTC 27 June (figure omitted). Differences in duct distribution with and without sea spray appear in the northeast and southwest directions of the Taiwan Region, the west of Philippines, and the southeast part of the model domain. Typhoon ducts are more susceptible to the effect of sea spray when

they are closer to the typhoon center, and with the increase of typhoon intensity, the influence range of sea spray is also increased. Besides, comparison between Figs. 4 and 7 indicates that the WRF model is less capable to forecast the associated duct distribution for a much stronger typhoon.

4.2.3 Duct structure

To further investigate the effect of sea spray on typhoon duct structure, the M profiles from EXP-2 and EXP-3 together with the GPS dropsonde mea-

surements are compared in Fig. 8. It is shown that sea spray mainly affects the duct strength and thickness, but the effects are not significant. The sea spray effects may cause typhoon duct to strengthen and can also cause it to weaken.

4.2.4 Cause analysis

The above analyses lead to a preliminary conclusion that sea spray exerts a certain impact on the distribution and structure of typhoon duct, but its impact is not significant, which turns out to be different from

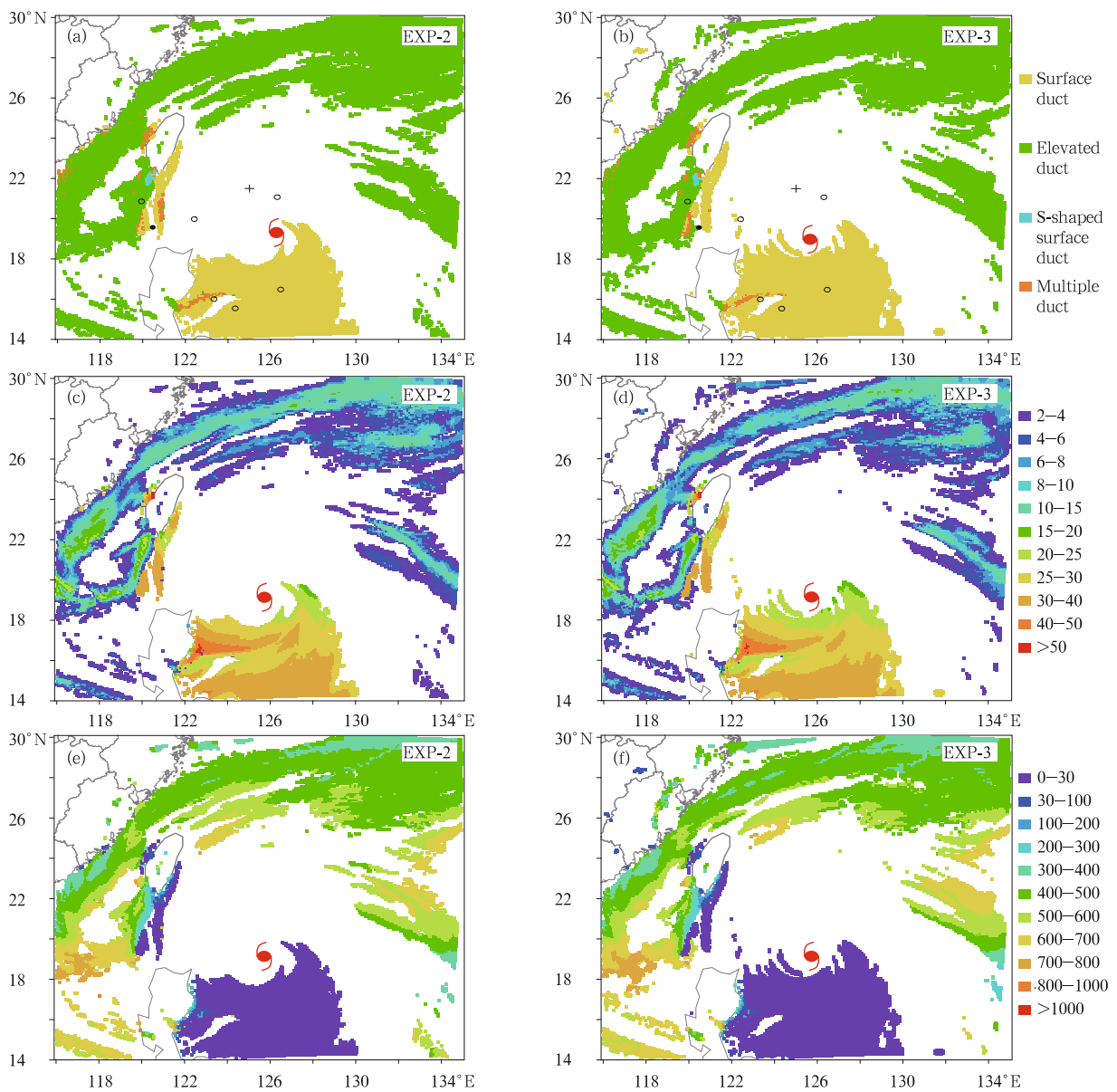


Fig. 7. As in Fig. 4, but for EXP-2 and EXP-3 at 1200 UTC 28 June. Plus signs indicate multiple ducts composed of surface duct and elevated duct; other symbols are the same as in Fig. 4.

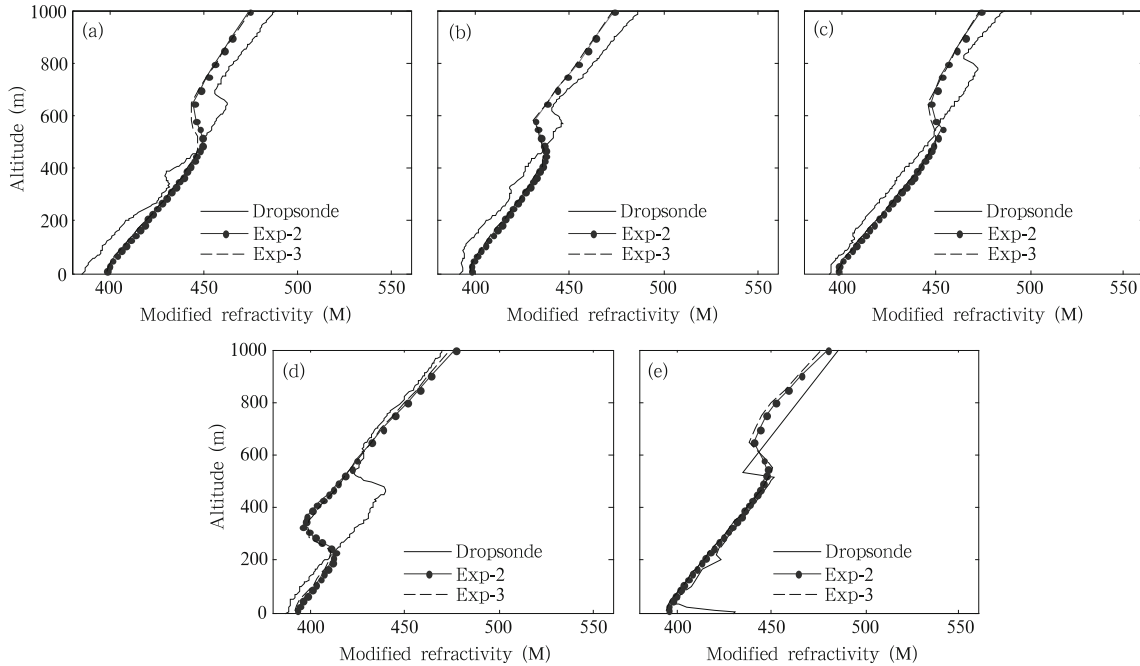


Fig. 8. As in Fig. 5, but for EXP-2 and EXP-3 versus the GPS dropsonde measurements.

our expectation and inspires us to further analyze the underlying reason.

In a mesoscale numerical model, sea spray participates in the air-sea interactions by the form of spray sensible and latent heat fluxes. To reveal the impact of sea spray on surface sensible and latent heat fluxes as well as its influence area, we analyze the distributions of enthalpy flux and 10-m wind speed within

360 km around the typhoon center, with and without sea spray, at 1200 UTC 28 June (Fig. 9), together with the radial distribution of azimuthally averaged heat flux difference, including sensible heat (SH), latent heat (LH), and enthalpy (EH) fluxes (Fig. 10). As shown in Fig. 9, the differences of wind speed and enthalpy flux, with and without sea spray, are concentrated at the maximum wind speed area near the

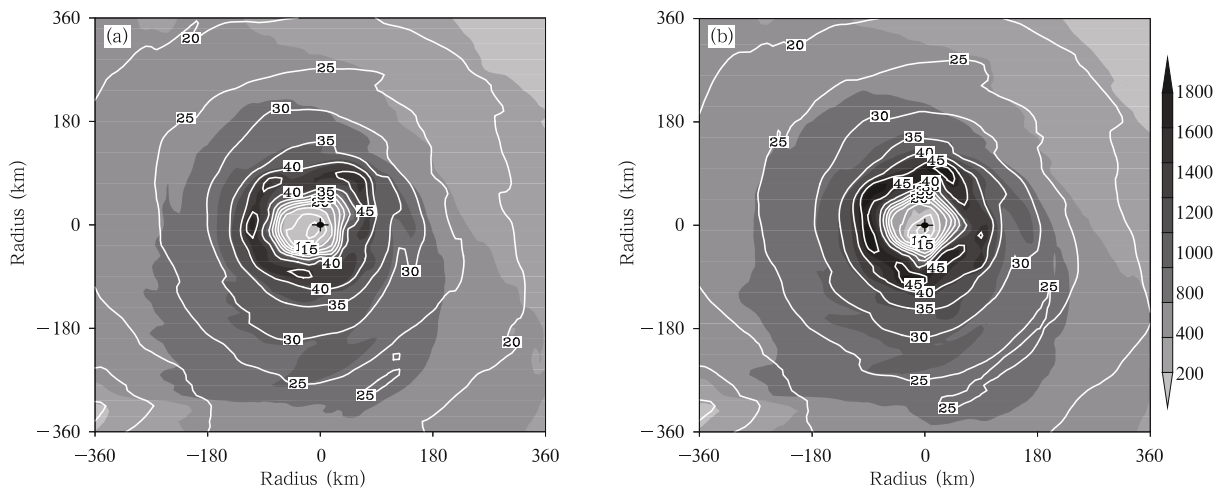


Fig. 9. Distributions of enthalpy flux (shaded; $W m^{-2}$) and 10-m wind speed (contour; $m s^{-1}$) within 360 km around the typhoon center from (a) EXP-2 and (b) EXP-3 at 1200 UTC 28 June. Note that the center of each panel indicates the typhoon center.

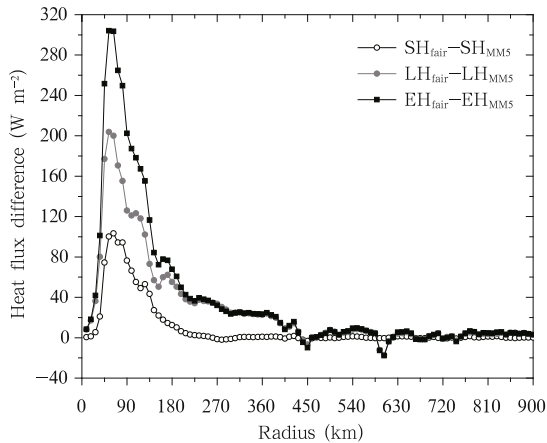


Fig. 10. Radial distribution of the azimuthally averaged sensible heat (SH), latent heat (LH), and enthalpy (EH) flux differences (EXP-3 minus EXP-2) at 1200 UTC 28 June.

typhoon center. After taking into account of sea spray's contribution, the large heat flux area (greater than 1600 W m^{-2}) and the maximum wind region (more than 45 m s^{-1}) from EXP-3 are enlarged significantly around the typhoon center. The maximal enthalpy flux and 10-m wind speed are increased by about 300 W m^{-2} and 5 m s^{-1} in EXP-3, respectively, compared to those in EXP-2 without sea spray.

The influence range of sea spray is explicitly shown in Fig. 10. We can see that the impacts of sea spray are significant at 1200 UTC 28 June, especially in the maximum wind speed area (about 90 km away from the typhoon center) where surface heat fluxes are significantly enhanced by sea spray with the maximal increase up to 300 W m^{-2} or so, in which latent heat flux has made a major contribution. It is also found that the impacts of sea spray are significantly weakened with the increase of radial distance. Specifically, the influence range of sea spray on sensible heat flux is 270 km or so, but it is extended to about 630 km for latent heat flux.

Therefore, beyond 270 km from the TC center, sea spray affects the distribution and structure of typhoon ducts mainly by changing the latent heat flux at the air-sea interface, which changes the upward transport of heat and moisture, resulting the changes of temperature and humidity structures in the bound-

ary layer. However, the impacts of sea spray on air-sea heat flux are concentrated at the maximum wind speed area near the typhoon center; with the increase of radial range, the effects are significantly weakened. This is the main reason why the impacts of sea spray on typhoon ducts are not very obvious.

Here, a case study is carried out to further investigate how sea spray impacts the characteristics of typhoon ducts. Taking the duct event located at 18.6°N , 120.3°E about 285 km southwest of the typhoon center at 1049 UTC 29 June (see Fig. 8e) for instance, the simulated elevated duct is enhanced from 7.5 (without sea spray) to 12.7 M (with sea spray), and the latter is much closer to the observation. Note, for this case, the impacts of sea spray on duct thickness and height are insignificant.

To investigate how sea spray enhances the duct strength, we analyze the azimuthally averaged heat flux differences and the boundary layer water vapor and potential temperature differences (EXP-3 minus EXP-2), with (EXP-3) and without (EXP-2) sea spray during 66–72-h integration, since 1049 UTC 29 June is just within this period and the feedbacks of sensible and latent heat fluxes to the ambient environment may need a response time. Here, we emphasize the area beyond 270 km from the typhoon center, because in this case the duct is located at 285 km away southwest of the TC center. As shown in Fig. 11, the average contribution of sea spray to latent heat flux is only 20.4 W m^{-2} in the range 270–360 km from the typhoon center, whereas the average contribution to sensible heat flux within this range is nearly zero. Therefore, the impacts of sea spray on the boundary layer temperature and humidity are very weak with the maximum difference of only ± 0.1 . It is noteworthy that the atmosphere above the altitude of 700–1000 m about 270 km away from the typhoon center is warm and dry, considering the spray effects; whereas the atmosphere under this level is cool and moist, resulting in an intensification of temperature inversion and a sharper decrease of moisture with height there. This is the direct reason for sea spray to enhance the duct strength. The simulated water vapor mixing ratio and potential temperature profiles for this duct case with (EXP-3)

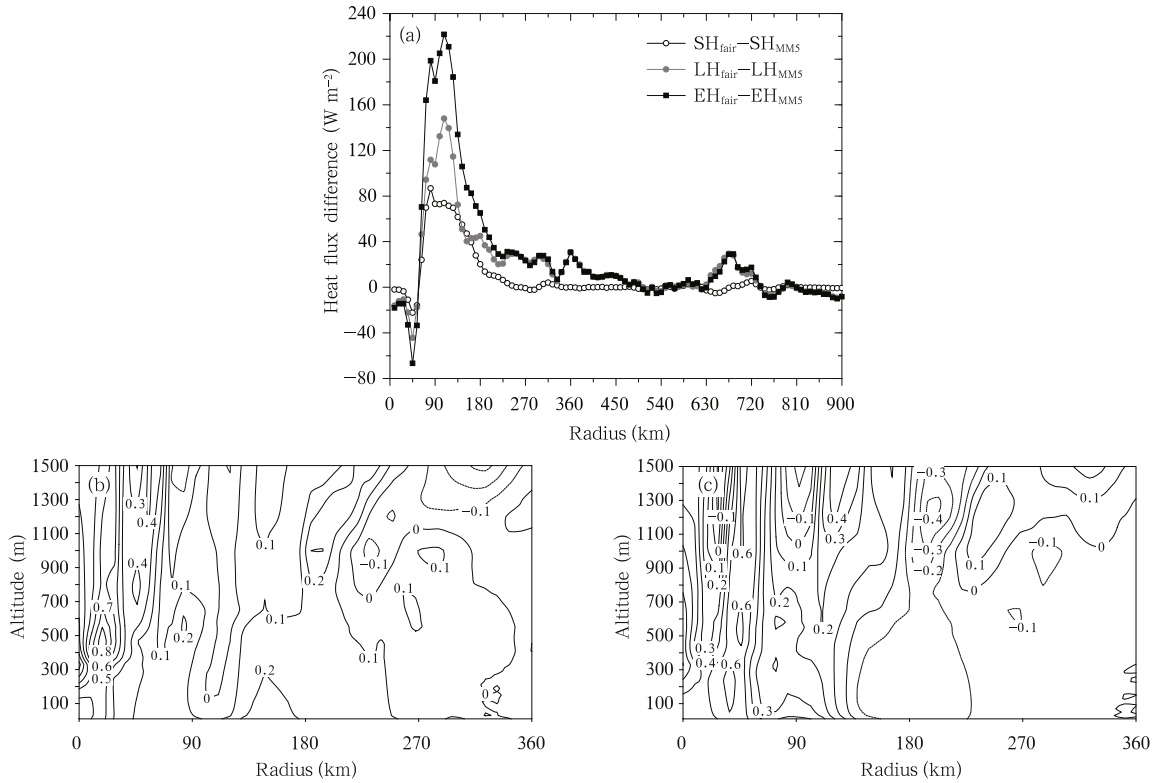


Fig. 11. (a) Radial distribution of the azimuthally averaged heat flux difference; and radial-vertical cross-sections of the azimuthally averaged differences (EXP-3 minus EXP-2) of (b) water vapor mixing ratio (g kg^{-1}) and (c) potential temperature (K) during 66–72 h.

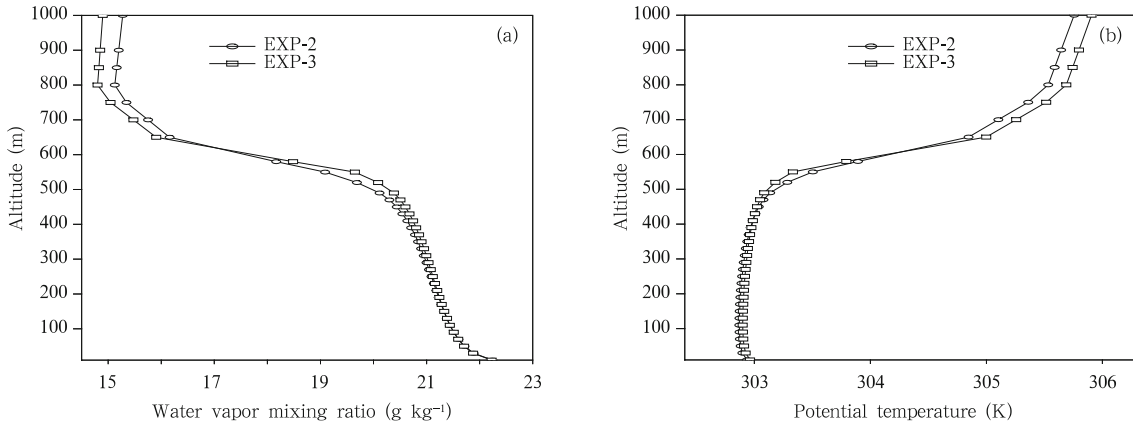


Fig. 12. Profiles of (a) water vapor mixing ratio (g kg^{-1}) and (b) potential temperature (K) at 18.6°N , 120.3°E from EXP-2 and EXP-3 at 1100 UTC 29 June.

and without (EXP-2) sea spray are compared in Fig. 12, which also verifies the above analysis.

Note that the effect of sea spray is generally to moisten the boundary layer, but its impact on temperature depends on the total amount of spray and

the relative position of spray to the typhoon center (Gall et al., 2008). The typhoon duct may be enhanced if the boundary layer under this duct is cooled and moistened by sea spray, otherwise it may be weakened.

5. Conclusions and discussion

A ducting process induced by Typhoon Mindule (2004) was simulated with the WRF model (version 3.2). The impacts of the bogus data assimilation (BDA) scheme and sea spray parameterization (SSP) on the simulation of typhoon ducts were analyzed. The results show that typhoon ducts are likely to form in every direction around the typhoon center, with the main type of ducts being elevated duct. Improved typhoon intensity forecast by the BDA scheme favors the correct simulation of duct structure and distribution. Sea spray affects typhoon ducts beyond 270 km from typhoon center mainly by changing the latent heat flux at the air-sea interface, which consequently changes the upward transport of heat and moisture, resulting in the changes of temperature and humidity structures in the boundary layer. Generally, the effect of sea spray is to moisten the boundary layer, but its influence on temperature depends on the total amount of spray and the relative position of spray to the typhoon center. If the boundary layer is cooled and moistened by sea spray, the typhoon duct strength may be enhanced, otherwise it may be weakened. However, the impacts of sea spray on typhoon duct are not very obvious, because the sea spray impacts on air-sea heat flux are concentrated in the maximum wind speed area near the typhoon center, with the increase of radial range, the impacts are significantly weakened.

Our previous study (Ding et al., 2013) shows that the distribution of typhoon ducts is associated with the variation of typhoon intensity. The present study has further revealed that improved typhoon intensity forecast by the BDA scheme can exert a positive effect on typhoon duct simulation.

By comparing the model results to the GPS dropsonde observations, we find that the WRF v3.2 indeed has the capability of forecasting typhoon duct distribution and structure, but it becomes less capable for stronger TCs, especially when the ducts are close to the typhoon center. This is one of the most challenging problems for typhoon duct forecasting and research, and our future study will be targeted along

this direction.

Acknowledgments. The authors wish to thank Professor Wu Junjie and others in “DOTSTAR” for providing the GPS dropsonde data. We are very grateful to the reviewers of this article for their insightful comments and suggestions.

REFERENCES

- Atkinson, B. W., J. G. Li, and R. S. Plant, 2001: Numerical modeling of the propagation environment in the atmospheric boundary layer over the Persian Gulf. *J. Appl. Meteor.*, **40**(3), 586–603.
- Bean, B. R., and E. J. Dutton, 1968: *Radio Meteorology*. Dover, New York, 435 pp.
- Chang, P. L., and P. F. Lin, 2011: Radar anomalous propagation associated with foehn winds induced by Typhoon Krosa (2007). *J. Appl. Meteor. Climatol.*, **50**(7), 1527–1542.
- Chen, F., and J. Dudhia, 2001: Coupling an advanced land surface-hydrology model with the Penn State-NCAR MM5 modeling system. Part I: Model implementation and sensitivity. *Mon. Wea. Rev.*, **129**(4), 569–585.
- Cheng Yinhe, 2009: A study on atmospheric ducts over the sea retrieval with AMSR-E satellite data and its numerical simulation. Ph. D. dissertation, Chinese Academy of Sciences, 101 pp. (in Chinese)
- Cook, J., 1991: A sensitivity study of weather data inaccuracies on evaporation duct height algorithms. *Radio Sci.*, **26**(3), 731–746.
- Ding Juli, Fei Jianfang, Huang Xiaogang, et al., 2013: Observational occurrence of tropical cyclone ducts from GPS dropsonde data. *J. Appl. Meteor. Climatol.*, **52**(5), 1221–1236.
- Dockery, G. D., 1988: Modeling electromagnetic wave propagation in the troposphere using the parabolic equation. *IEEE Trans. Antennas Propag.*, **36**(10), 1464–1470.
- Dudhia, J., 1989: Numerical study of convection observed during the winter monsoon experiment using a mesoscale two-dimensional model. *J. Atmos. Sci.*, **46**(20), 3077–3107.
- Fairall, C. W., J. D. Kepert, and G. J. Holland, 1994: The effect of sea spray on surface energy transports over the ocean. *Global Atmos. Ocean Syst.*, **2**, 121–142.
- Gall, J. S., W. M. Frank, and Y. Kwon, 2008: Effects of sea spray on tropical cyclones simulated under

- idealized conditions. *Mon. Wea. Rev.*, **136**(5), 1686–1705.
- Hong, S. Y., Y. Noh, and J. Dudhia, 2006: A new vertical diffusion package with an explicit treatment of entrainment processes. *Mon. Wea. Rev.*, **134**(9), 2318–2341.
- Hu Xiaohua, Fei Jianfang, Li Juan, et al., 2007: Analysis and numerical simulation research of atmospheric duct affected by typhoon. *Marine Forecasts*, **24**(2), 17–25. (in Chinese)
- Kain, J. S., 2004: The Kain-Fritsch convective parameterization: An update. *J. Appl. Meteor.*, **43**(1), 170–181.
- , and J. M. Fritsch, 1990: A one-dimensional entraining/detraining plume model and its application in convective parameterization. *J. Atmos. Sci.*, **47**(23), 2784–2802.
- Lin, Y. L., R. D. Farley, and H. D. Orville, 1983: Bulk parameterization of the snow field in a cloud model. *J. Climate Appl. Meteor.*, **22**(6), 1065–1092.
- Liu Chengguo, Huang Jiying, and Jiang Changyin, 2002: The occurrence of tropospheric ducts over the south-eastern coast of China. *Chin. J. Radio Sci.*, **17**(5), 509–513. (in Chinese)
- Liu Guiyan, Gao Shanhong, Wang Yongming, et al., 2012: Numerical simulation of atmospheric duct in typhoon subsidence area. *J. Appl. Meteor. Sci.*, **23**(1), 77–88. (in Chinese)
- Mesnard, F., and H. Sauvageot, 2010: Climatology of anomalous propagation radar echoes in a coastal area. *J. Appl. Meteor. Climatol.*, **49**(11), 2285–2300.
- Mlawer, E. J., S. J. Taubman, P. D. Brown, et al., 1997: Radiative transfer for inhomogeneous atmospheres: RRTM, a validated correlated- k model for the long-wave. *J. Geophys. Res.*, **102**(D14), 16663–16682.
- Pan Zhongwei, Liu Chengguo, and Guo Li, 1996: The prediction of ducts on the south-east coast of China. *Chin. J. Radio Sci.*, **11**(3), 58–64. (in Chinese)
- Parrish, D. F., and J. C. Derber, 1992: The National Meteorological Center's spectral statistical interpolation analysis system. *Mon. Wea. Rev.*, **120**(8), 1747–1763.
- Rutledge, S. A., and P. V. Hobbs, 1984: The mesoscale and microscale structure and organization of clouds and precipitation in midlatitude cyclones. XII: A diagnostic modeling study of precipitation development in narrow cold-frontal rainbands. *J. Atmos. Sci.*, **41**(20), 2949–2972.
- Turton, J. D., D. A. Bennets, and S. F. G. Farmer, 1988: An introduction to radio ducting. *Meteor. Mag.*, **117**, 245–254.
- Xiao, Q. N., X. L. Zou, and B. Wang, 2000: Initialization and simulation of a landfalling hurricane using a variational bogus data assimilation scheme. *Mon. Wea. Rev.*, **128**(7), 2252–2269.
- , L. Q. Chen, and X. Y. Zhang, 2008: Evaluations of BDA scheme using the Advanced Research WRF (ARW) model. *J. Appl. Meteor.*, **48**(3), 680–689.
- Zheng Jing, Fei Jianfang, Du Tao, et al., 2008: Effect of sea spray on the numerical simulation of super Typhoon “Ewiniar”. *J. Ocean Univ. China*, **7**(4), 362–372.
- Zou, X. L., and Q. N. Xiao, 2000: Studies on the initialization and simulation of a mature hurricane using a variational bogus data assimilation scheme. *J. Atmos. Sci.*, **57**(6), 836–860.